

Channel selection for multispectral color imaging using binary differential evolution

Hui-Liang Shen,^{1,*} Jian-Fan Yao,¹ Chunguang Li,¹ Xin Du,¹
Si-Jie Shao,² and John H. Xin²

¹Department of Information Science and Electronic Engineering, Zhejiang University, Hangzhou 310027, China

²Institute of Textiles and Clothing, The Hong Kong Polytechnic University, Hong Kong, China

*Corresponding author: shenhl@zju.edu.cn

Received 21 October 2013; accepted 13 December 2013;
posted 18 December 2013 (Doc. ID 199857); published 24 January 2014

In multispectral color imaging, there is a demand to select a reduced number of optimal imaging channels to simultaneously speed up the image acquisition process and keep reflectance reconstruction accuracy. In this paper, the channel selection problem is cast as the binary optimization problem, and is consequently solved using a novel binary differential evolution (DE) algorithm. In the proposed algorithm, we define the mutation operation using a differential table of swapping pairs, and deduce the trial solutions using neighboring self-crossover. In this manner, the binary DE algorithm can well adapt to the channel selection problem. The proposed algorithm is evaluated on the multispectral color imaging system on both synthetic and real data sets. It is verified that high color accuracy is achievable by only using a reduced number of channels using the proposed method. In addition, as binary DE is a global optimization algorithm in nature, it performs better than the traditional sequential channel selection algorithm. © 2014 Optical Society of America

OCIS codes: (110.4234) Multispectral and hyperspectral imaging; (330.1730) Colorimetry; (330.1710) Color, measurement.

<http://dx.doi.org/10.1364/AO.53.000634>

1. Introduction

In recent years, multispectral color imaging has attracted intensive interest, as it can acquire more spectral information than traditional RGB cameras. Equipped with filters, a multispectral camera captures spectral images under natural illumination conditions, by splitting the visible spectrum into more than three bands. A multispectral imaging system can be set up by using a monochrome camera and electronically controlled acousto-optic or liquid-crystal tunable filters [1,2]. Figure 1 illustrates an alternative multispectral imaging system that consists of a monochrome camera and a filter wheel. The filter wheel, which contains a number of filters, is installed between the camera and

the lens. When the imaging system has been calibrated and characterized, the spectral reflectance data of the imaged sample can be obtained at pixel-level resolution [2,3]. Because of its advantages, multispectral color imaging has been widely applied in various areas such as scene simulation [4], digital archiving [5], and spectral color measurement [2,6].

In multispectral color imaging, the spectral reflectance can be reliably reconstructed from camera responses using typical techniques, such as Wiener estimation [5], pseudo-inverse [7], and finite-dimensional modeling [8]. Considering that the spectral characteristics of filters (or sensors) could affect the reconstruction accuracy [9], some works have addressed the optimal design of filters. For example, Shimano [10] investigated the optimal design of Gaussian spectral sensitivities of sensors in the presence of imaging noise, while Lopez-Alvarez *et al.* [11]

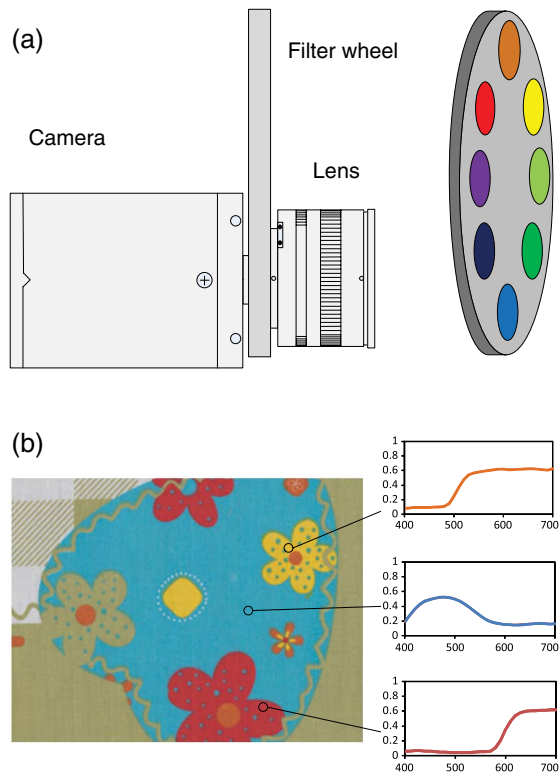


Fig. 1. (a) Schematic multispectral imaging system that consists of a monochrome camera and a filter wheel. The filter wheel contains a number of filters. (b) Multispectral image (displayed in RGB format) from which the spectral reflectance for any pixel can be obtained.

dealt with a similar problem in the estimation of spectral skylights.

It is known that using a large number of filters can increase color accuracy [2], but this will, in turn, slow down the image acquisition process. From a practical perspective, there is a demand to select an optimal subset of imaging channels to balance the imaging efficiency and color accuracy. However, the works on this issue are quite limited, and the most relevant work may be that of Hu and Wu [12]. They proposed a sensor selection method in the representation of daylight spectra. They first sequentially selected 15 sensors from 30 ones according to a correlation criterion, and then chose six optimal sensors from the 15 by exhaustive search.

Actually, channel selection is similar to the problem of color selection in imaging device characterization. In this area, Hardeberg [7] introduced a method for significant color selection using a minimum condition number to estimate the spectral sensitivity of the camera. Cheung and Westland [13] proposed several metric formulas to select optimal colors for colorimetric characterization based on the assumption that the current selected color should be as different as possible from those already selected. Shen *et al.* [14] also introduced a color selection method by minimizing the reflectance reconstruction error of a virtual imaging system. Note that these methods all select colors in a sequential manner

and thus can only produce suboptimal solutions. Alternatively, Alsam and Finlayson [15] cast the color selection problem as a quadratic minimization problem and solved it using integer programming. A limitation of this work is that, as the objective function is the cross-product matrix of reflectance, the obtained solution may still not be optimal for reflectance reconstruction.

In this paper we convert the optimal channel selection problem to a binary optimization problem, and solve it using a differential evolution (DE) algorithm. The original DE algorithm, which is introduced by Price and Storn [16,17], conducts optimization in continuous search spaces. Recently, Prado *et al.* [18] proposed a general discrete DE algorithm for combinatorial optimization, and Kashan *et al.* [19] introduced a binary version of the DE algorithm. We propose a binary DE algorithm that is suitable to our channel selection problem, by defining novel binary mutation and crossover operations. The performance of the proposed algorithm is evaluated on the multispectral imaging system with both synthetic and real data.

2. Imaging Model

As illustrated in Fig. 1, the multispectral imaging system consists of a monochrome camera and a set of filters. Without loss of generality, we suppose the visible spectrum, from 400 to 700 nm, is sampled into $N = 31$ samples at a 10 nm interval. Let $s(\lambda)$ be the spectral sensitivity of the camera, $f_c(\lambda)$ the spectral transmittance of the filter at channel $c \in \{1, 2, \dots, C\}$, $l(\lambda)$ the spectral power distribution of the illuminant, and $r(\lambda)$ the spectral reflectance of the object surface; then the camera responses q_c are formulated as [2]

$$q_c = \sum_{\lambda=1}^N l(\lambda) f_c(\lambda) s(\lambda) r(\lambda) + n_c = \sum_{\lambda=1}^N m(\lambda) r(\lambda) + n_c, \quad (1)$$

where n_c denotes imaging noise. For simplicity, we use the spectral responsivity term $m_c(\lambda) = l(\lambda) f_c(\lambda) s(\lambda)$ to combine the optical characteristics of the illuminant, filter, and camera.

In matrix-vector notation, Eq. (1) is written as

$$q_c = \mathbf{m}_c^T \mathbf{r} + n_c, \quad (2)$$

where \mathbf{m}_c denotes the column vector of spectral responsivity of channel c , and \mathbf{r} denotes the reflectance vector. By considering all the C channels together, the response vector $\mathbf{q} = (q_1, q_c, \dots, q_C)^T$ is

$$\mathbf{q} = \mathbf{M} \mathbf{r} + \mathbf{n}, \quad (3)$$

where \mathbf{n} denotes the noise vector. The spectral responsivity matrix \mathbf{M} is denoted as

$$\mathbf{M} = (\mathbf{m}_1, \mathbf{m}_2, \dots, \mathbf{m}_C)^T, \quad (4)$$

or explicitly expressed as

$$\mathbf{M} = \begin{pmatrix} m_1(1) & m_1(2) & \cdots & m_1(N) \\ m_2(1) & m_2(2) & \cdots & m_2(N) \\ \cdots & \cdots & \cdots & \cdots \\ m_C(1) & m_C(2) & \cdots & m_C(N) \end{pmatrix}. \quad (5)$$

The responsivity matrix \mathbf{M} can be mathematically obtained when the camera responses and reflectance data of a set of color samples are available. A natural constraint in the computation is that its values should be non-negative,

$$m_c(\lambda) \geq 0. \quad (6)$$

In the case of wideband filters, the smoothness constraint should be further satisfied,

$$|2m_c(\lambda) - m_c(\lambda - 1) - m_c(\lambda + 1)| < \delta, \quad (7)$$

where δ denotes the constant parameter that controls the smoothness degree.

With the estimated \mathbf{M} , the noise variance of channel c is computed as

$$\sigma_c^2 = E\{\|q_c - \mathbf{m}_c^T \mathbf{r}\|^2\}, \quad (8)$$

which can be further used in reflectance reconstruction.

3. Problem Statement

An important issue in multispectral imaging is to reconstruct spectral reflectance with high color accuracy. Mathematically, this is to find a reconstruction matrix \mathbf{W} such that the spectral reflectance can be estimated from camera response \mathbf{q} ,

$$\hat{\mathbf{r}} = \mathbf{W}\mathbf{q}. \quad (9)$$

The reconstruction matrix \mathbf{W} can be obtained using various techniques, such as constrained least squares. In this paper we employ the well-known Wiener estimation [2,5],

$$\mathbf{W} = \mathbf{K}_r \mathbf{M}^T (\mathbf{M} \mathbf{K}_r \mathbf{M}^T + \mathbf{K}_n)^{-1}, \quad (10)$$

where \mathbf{K}_r is the autocorrelation matrix of reflectance, and \mathbf{K}_n is a diagonal matrix, $\mathbf{K}_n = \text{diag}\{\sigma_1^2, \sigma_2^2, \dots, \sigma_C^2\}$. As can be seen from Eq. (10), the computation of reconstruction matrix \mathbf{W} is based on the spectral responsivity and noise variance of the imaging system.

Note that the matrix \mathbf{W} in Eq. (10) is computed on the full channel set $\Omega_{\text{FULL}} = \{1, 2, \dots, C\}$. When only a subset of channels, $\Omega \subset \Omega_{\text{FULL}}$, is used, it becomes

$$\mathbf{W}_\Omega = \mathbf{K}_r \mathbf{M}_\Omega^T (\mathbf{M}_\Omega \mathbf{K}_r \mathbf{M}_\Omega^T + \mathbf{K}_{n,\Omega})^{-1}. \quad (11)$$

Here, spectral responsivity submatrix \mathbf{M}_Ω is constructed by the rows of \mathbf{M} specified by Ω , and the noise submatrix $\mathbf{K}_{n,\Omega}$ is constructed similarly.

Practically, it is required that high spectral accuracy can still be kept when only a reduced number, C_S , of imaging channels is employed. Mathematically, this is to find the channel subset Ω that minimizes the following expected spectral error:

$$f(\Omega) = E\{\|\mathbf{r} - \mathbf{W}_\Omega \mathbf{u}\|^2\} \\ = E\{\|\mathbf{r} - \mathbf{K}_r \mathbf{M}_\Omega^T (\mathbf{M}_\Omega \mathbf{K}_r \mathbf{M}_\Omega^T + \mathbf{K}_{n,\Omega})^{-1} \mathbf{q}\|^2\}, \quad (12)$$

which is actually the objective cost function of the channel selection problem.

4. Related Arts

The work dealing with the channel selection problem is quite limited. In this section, we first introduce the sequential channel selection algorithm, and then briefly review the basic DE algorithms for optimization purposes. The sequential algorithm will be used as the baseline method in the experiment.

A. Sequential Channel Selection

The imaging channels are selected one by one in the sequential method. The first channel is selected by

$$c_1 = \arg \min_c f(\{c\}), \quad c \in \Omega_{\text{FULL}}, \quad (13)$$

and consequently $\Omega \leftarrow \{c_1\}$. Then the following process iterates until all the C_S channels are selected:

$$c_k = \arg \min_c f(\Omega \cup \{c\}), \quad c \in \Omega_{\text{FULL}} \setminus \Omega, \quad (14)$$

and the channel subset is updated as $\Omega \leftarrow \Omega \cup \{c_k\}$.

We note that, as the objective function $f(\Omega)$ is not convex, the sequentially determined channels are only locally optimal. In this regard, a global optimization algorithm is needed to determine the subset Ω .

B. Basic Differential Evolution

DE [17] is powerful stochastic optimization algorithm over continuous search spaces. Most recently, it has been successfully applied in the characterization of desktop color printers [20].

DE generally consists of three operations, i.e., mutation, crossover, and selection. It starts with a random initialization of a population of individuals, and then works based on the evolution of individuals in the population. We outline the basic strategy for the continuous optimization problem in the following.

Let N_P be the number of individuals in the population, and G the maximum generation; then $\mathbf{x}_{g,i}$ denotes the i th individual in the g th generation. In the mutation operation, a new individual $\mathbf{v}_{g,i}$ is generated by adding the weighted difference between two randomly chosen individuals to a third one,

$$\mathbf{v}_{g,i} = \mathbf{x}_{g,r_1} + F(\mathbf{x}_{g,r_2} - \mathbf{x}_{g,r_3}), \quad (15)$$

where $r_1, r_2, r_3 \in \{1, 2, \dots, N_p\}$ are random mutually different indices, and $F \in (0, 1]$ is the scale factor applied to the differential vector. For each individual $\mathbf{x}_{g,i}$ a mutual vector $\mathbf{v}_{g,i}$ is generated.

In the crossover operation, a trial vector $\mathbf{u}_{g,i}$ is formed by the recombination of $\mathbf{x}_{g,i}$ and $\mathbf{v}_{g,i}$ with a probability p_c ,

$$\mathbf{u}_{g,i,d} = \begin{cases} \mathbf{v}_{g,i,d} & \text{if } \text{rand}() < p_c \\ \mathbf{x}_{g,i,d} & \text{otherwise} \end{cases}, \quad (16)$$

where the function $\text{rand}()$ generates a random number in range $[0, 1]$, and $\mathbf{u}_{g,i,d}$ are the d th elements of $\mathbf{u}_{g,i}$. The terms $\mathbf{v}_{g,i,d}$ and $\mathbf{x}_{g,i,d}$ are defined in a similar manner.

In the selection operation, the trial vector $\mathbf{u}_{g,i}$ competes with the current solution $\mathbf{x}_{g,i}$ using the cost evaluation. If the trial vector is better than the current vector in terms of cost value, it passes through the next generation; otherwise the current vector survives. This process is mathematically described as

$$\mathbf{x}_{g+1,i} = \begin{cases} \mathbf{u}_{g,i} & \text{if } f(\mathbf{u}_{g,i}) < f(\mathbf{x}_{g,i}) \\ \mathbf{x}_{g,i} & \text{otherwise} \end{cases}, \quad (17)$$

where $f(\cdot)$ is the cost function, which is of the form of Eq. (12) in this work.

The DE algorithm described above is only originally introduced for continuous optimization problems. As the mutation in Eq. (15) is based on the vector difference, the DE algorithm cannot be directly applied in binary optimization problems. To cope with this situation, Pampara *et al.* [21] perform optimization in binary spaces by using an angle modulation strategy without affecting the basic fundamentals of DE. The angle modulation provides a mechanism that maps a continuous search space to a binary space. Kashan *et al.* [19] introduce a binary DE algorithm by using the measure of dissimilarity between binary vectors. Its characteristic is that the algorithm works in continuous space while the consequence is used in binary space. A common drawback of these works is that, by default, they cannot keep the number of bit value 1 fixed in the solution vector, which in turn cannot be applied to our channel selection problem. In contrast, the proposed binary DE algorithm works in binary search spaces directly.

5. Proposed Channel Selection Algorithm

In this section, we cast the channel selection problem as a binary optimization problem, and then solve it using a novel binary DE algorithm that well adapts to our problem. Finally we list the DE algorithm for channel selection and discuss the related issues such as parameter setting and convergence property.

A. Problem Definition

As mentioned above, our objective is to select C_S imaging channels from a total number of C channels. To convert it to a binary optimization problem, we

define a binary solution vector \mathbf{x} containing C bits, which may have the following form:

$$\mathbf{x} = \underbrace{(0 \ 0 \ 1 \ 1 \ \dots \ 0 \ 1 \ 0 \ 1)}_{C \text{ bits}}. \quad (18)$$

In vector \mathbf{x} , the indices with bit value 1 indicate the selected channels, while those with bit value 0 indicate the unselected channels. The optimization problem is to determine a number (C_S) of indices of bit value 1 under the evaluation of the cost function (12).

B. Binary Differential Evolution

In binary optimization, the differential mutation cannot be directly applied as this does not produce a meaningful search direction in the binary space. For our specific problem, the number of bits 1 should be kept as C_S for the solution vectors in the evolution procedure. In this regard, we define the difference between two candidate solutions, \mathbf{x}_i and \mathbf{x}_j , as a differential table of swapping pairs with bit values 0 and 1,

$$T_{ij} = \mathbf{x}_i \ominus \mathbf{x}_j, \quad (19)$$

where the binary minus operator \ominus produces the indices of swapping pairs in T_{ij} .

In accordance with the continuous DE, we apply a constant scale $F \in (0, 1]$ to T_{ij} , which produces the scaled differential table

$$T_{ij}^F = F \otimes T_{ij}. \quad (20)$$

We treat F as a probability, and define the binary multiplication operator \otimes as the probabilistic selection of swapping pairs in T_{ij} .

With the above definitions, the mutation vector \mathbf{v}_k can be generated as

$$\mathbf{v}_k = \mathbf{x}_k \oplus F \otimes (\mathbf{x}_i \ominus \mathbf{x}_j) = \mathbf{x}_k \oplus F \otimes T_{ij} = \mathbf{x}_k \oplus T_{ij}^F, \quad (21)$$

where the binary plus operator \oplus swaps the bit values of the indices of \mathbf{x}_k according to the swapping pairs specified in table T_{ij}^F . As can be seen, the generation of the mutation vector is similar to that of continuous DE in Eq. (15).

In this work, a set of trial vectors are generated in a special manner such that the DE algorithm well adapts to our channel selection problem. First, the mutation vector itself is used as one trial vector. Then, additional trial vectors are generated by swapping the neighboring indices of the mutation vector. This operation will be referred as self-crossover in the following. Mathematically, the trial vectors are generated using a set of self-crossover differential tables T_{SC} ,

$$\mathbf{u}_k = \mathbf{v}_k \oplus T_{SC}, \quad (22)$$

where each T_{SC} contains a swapping pair of neighboring indices with different bit values.

In multispectral color imaging, considering the smooth characteristics of spectral reflectance, it is worthwhile to check whether exchanging neighboring channels can improve color measurement accuracy. This is implemented by generating trial vectors with the differential tables T_{SC} .

C. Numerical Example

We use a numerical example to illustrate the main operations of the binary DE algorithm. Suppose we have two candidate vectors with eight elements,

$$\begin{aligned} \mathbf{x}_i &= (0 \ 0 \ 1 \ 1 \ 0 \ 0 \ 1 \ 1), \\ \mathbf{x}_j &= (1 \ 1 \ 0 \ 0 \ 1 \ 0 \ 0 \ 1), \end{aligned}$$

both of which have four indices with bit value 1. Supposing the vector index starts from 1, the differential table T_{ij} is computed as

$$T_{ij} = \mathbf{x}_i \ominus \mathbf{x}_j = \begin{pmatrix} 1 & 2 & 5 \\ 3 & 4 & 7 \end{pmatrix},$$

in which (1,3), (2,4), and (5,7) are three swapping pairs.

With a probability $F \in (0, 1]$, the scaled differential table may become

$$T_{ij}^F = F \otimes T_{ij} = \begin{pmatrix} 1 & 5 \\ 3 & 7 \end{pmatrix},$$

in which we assume the second swapping pair (2, 4) in T_{ij} is removed. We note that, as the solution vector is of binary form, T_{ij}^F keeps the same swapping effect if we swap the two rows, or exchange the elements within each row. More explicitly, the following differential tables are equivalent for the proposed binary DE algorithm:

$$\begin{pmatrix} 1 & 5 \\ 3 & 7 \end{pmatrix} \sim \begin{pmatrix} 3 & 7 \\ 5 & 1 \end{pmatrix} \sim \begin{pmatrix} 1 & 5 \\ 7 & 3 \end{pmatrix} \sim \begin{pmatrix} 5 & 1 \\ 3 & 7 \end{pmatrix}.$$

Suppose that a third candidate solution vector is

$$\mathbf{x}_k = (1 \ 0 \ 0 \ 1 \ 0 \ 0 \ 1 \ 1).$$

By applying the differential table T_{ij}^F , the mutation vector becomes

$$\mathbf{v}_k = \mathbf{x}_k \oplus T_{ij}^F = (0 \ 0 \ 1 \ 1 \ 1 \ 0 \ 0 \ 1).$$

Checking the neighboring indices with bit patterns (0, 1) or (1, 0), \mathbf{v}_k produces three self-crossover differential tables:

$$T_{SC} = \begin{pmatrix} 2 \\ 3 \end{pmatrix}, \begin{pmatrix} 5 \\ 6 \end{pmatrix}, \begin{pmatrix} 7 \\ 8 \end{pmatrix}.$$

Consequently, in addition to the mutation vector, the set of trial vectors also includes

$$(0 \ 1 \ 0 \ 1 \ 1 \ 0 \ 0 \ 1),$$

$$(0 \ 0 \ 1 \ 1 \ 0 \ 1 \ 0 \ 1),$$

and

$$(0 \ 0 \ 1 \ 1 \ 1 \ 0 \ 1 \ 0).$$

D. Optimal Channel Selection

In our multispectral color imaging system, the total number of channels is $C = 16$, and the number of channels to be selected, $C_S \in \{3, 4, \dots, 16\}$. When $C_S = 3$, the multispectral imaging system becomes a traditional three-band camera. The determination of appropriate C_S value depends on the trade-off between channel reduction and color accuracy, as will be discussed in Section 6.

As mentioned above, the proposed binary DE algorithm adapts to the channel selection problem due to two reasons. First, the mutation vector produced by the differential table keeps the same number (C_S) of bit values 1. Second, the generation strategy of trial vectors enables the check of neighboring channels.

The pseudo code of the binary DE algorithm for optimal channel selection is listed in Algorithm 1.

Algorithm 1 Binary Differential Evolution

Parameters:

- N_P : Number of individuals
- F : Scaling constant
- G : Maximum generation

Initialization:

- Generate population $\{\mathbf{x}_{g,1}, \mathbf{x}_{g,2}, \dots, \mathbf{x}_{g,N_P}\}$

while stop criterion is not met **do**

for each $i \in \{1, 2, \dots, N_P\}$ **do**

- Select $r_2 \neq r_3 \in \{1, 2, \dots, N_P\} \setminus \{i\}$
- Generate mutant vector: $\mathbf{v}_{g,i} = \mathbf{x}_{g,i} \oplus F \otimes (\mathbf{x}_{g,r_2} \ominus \mathbf{x}_{g,r_3})$
- Generate trial vectors $\mathbf{u}_{g,i}$ from $\mathbf{v}_{g,i}$
- Find the best trial vector $\tilde{\mathbf{u}}_{g,i}$ by cost evaluation
- Perform competition between $\tilde{\mathbf{u}}_{g,i}$ and $\mathbf{x}_{g,i}$: $\mathbf{x}_{g+1,i} = \begin{cases} \tilde{\mathbf{u}}_{g,i} & \text{if } f(\tilde{\mathbf{u}}_{g,i}) < f(\mathbf{x}_{g,i}) \\ \mathbf{x}_{g,i} & \text{otherwise} \end{cases}$

end

$g \leftarrow g + 1$

end

Output: Optimal solution $\mathbf{x} = \arg \min f(\mathbf{x}_{g,i})$,

$i \in \{1, 2, \dots, N_P\}$;

Our investigation indicates that the performance of the binary DE algorithm is insensitive to the parameters. Based on the observation that the number of all possible channel combinations is $\binom{C}{C_S}$, N_P is determined as

$$N_P = \max \left\{ 4, \left[\left(\frac{C}{C_S} \right)^{1/3} \right] \right\}, \quad (23)$$

where the operator $[x]$ rounds variable x to its nearest integer. We set the maximum generation $G = 30$ and the scaling constant $F = 0.8$ in all the experiments.

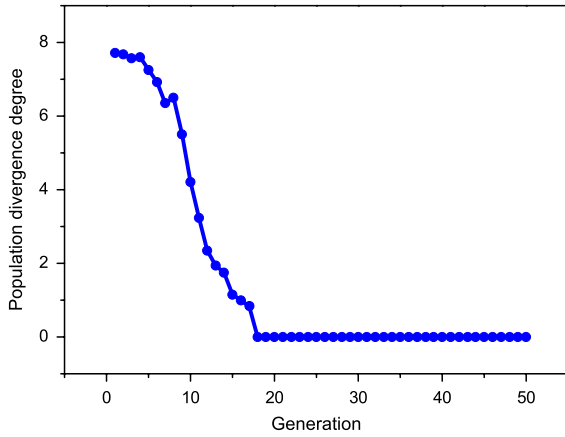


Fig. 2. Population diverse degree with respect to generation when the number of selected channels $C_S = 8$.

It is necessary to analyze the convergence property of Algorithm 1. In the initialization stage, the population is very diverse and the differential table contains a large number of swapping pairs. When evolution proceeds, the individuals will become more similar to each other, and the sizes of differential tables will consequently decrease. We compute the population diverse degree as

$$D = \frac{2}{N_p(N_p - 1)} \sum_{i=1}^{N_p} \sum_{j=i+1}^{N_p} \phi(x_i \odot x_j), \quad (24)$$

where \odot denotes the bit-wise XOR between two binary vectors, and the operator $\phi(\cdot)$ computes the number of bits with value 1. Figure 2 illustrates the variation trend of population diverse degree D with respect to generation g in the case of $C_S = 8$. It is clear that the individuals become similar to each other quickly after a number of generations, and remain stable afterward. Therefore the stop criterion in Algorithm 1 can be either g reaching G or $D \rightarrow 0$.

6. Experiments

The multispectral imaging system consists of a QImaging Retiga-EXi monochrome camera, OSRAM halogen tungsten lamps, a Nikkor lens with 50 mm fixed focal length, and $C = 16$ narrowband filters with 10 nm FWHM. The central wavelengths of these filters are at 400, 420, 440, ..., and 700 nm. To evaluate the proposed channel selection method intensively, we additionally simulate a multispectral imaging system using synthetic filters with various FWHM values as shown in Fig. 3(c). We use 144 randomly selected Pantone textile samples in the experiment, whose reflectance curves are illustrated in Fig. 3(d).

The color accuracy is evaluated using both colorimetric and spectral errors. The colorimetric error is computed using the CIEDE2000 color difference formula [22] under CIE standard illuminants D65, A, and F2. The spectral error is the root-mean-square (rms) error computed as

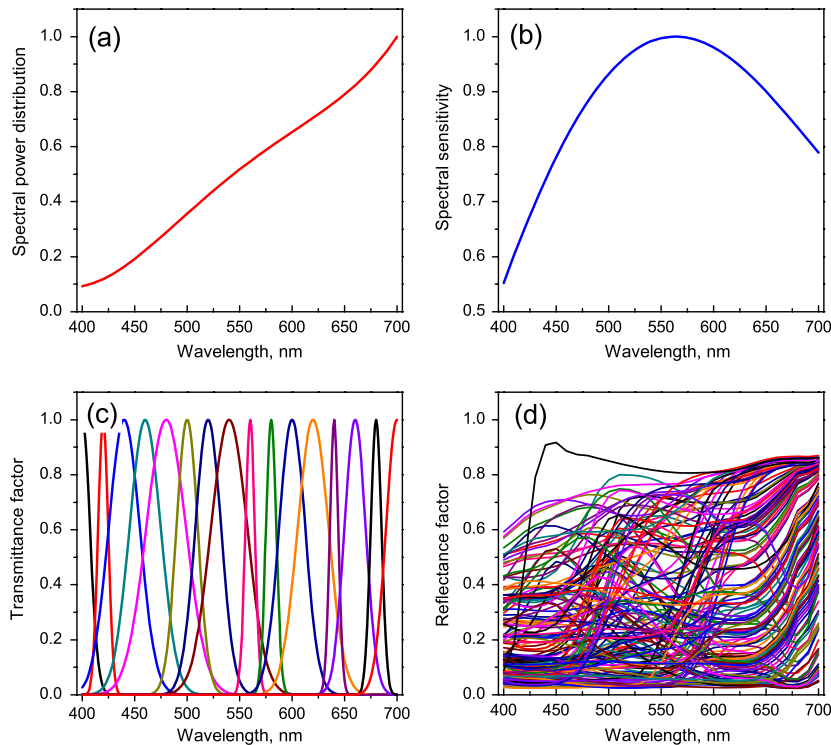


Fig. 3. Data of synthetic imaging system. (a) Spectral power distribution of the halogen tungsten lamps, (b) spectral sensitivity of the monochrome camera, (c) spectral transmittances of 16 synthetic filters with various full width at half-maximum (FWHM) values, and (d) spectral reflectance curves of 144 Pantone patches.

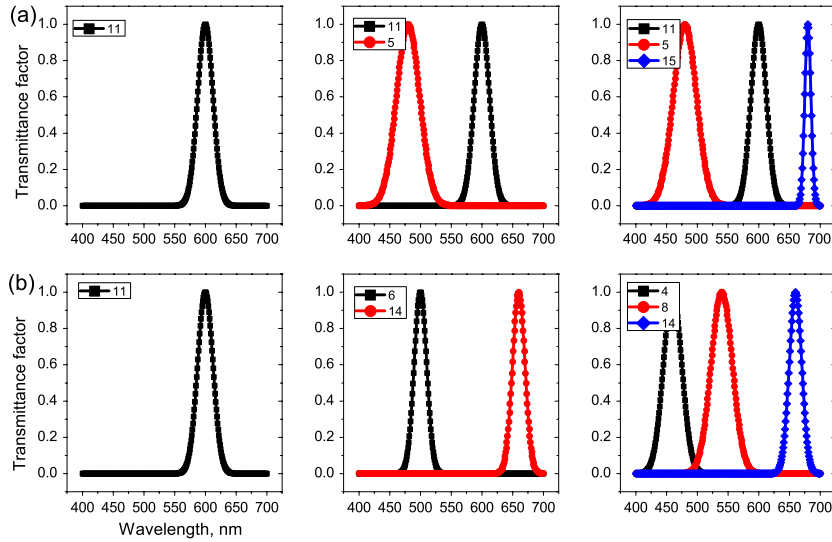


Fig. 4. Selected imaging channels when $C_S = 1, 2,$ and 3 . (a) Sequential algorithm. (b) Proposed binary DE algorithm.

$$\text{rms} = \left(\frac{1}{N} (\mathbf{r} - \hat{\mathbf{r}})^T (\mathbf{r} - \hat{\mathbf{r}}) \right)^{\frac{1}{2}}, \quad (25)$$

where $N = 31$ is the number of sampling points in the visible wavelength range, and \mathbf{r} and $\hat{\mathbf{r}}$ denote the ground truth and reconstructed reflectances, respectively.

A. Synthetic Data

Figure 3 illustrates the spectral power distribution of the halogen tungsten lamps and the spectral sensitivity of the monochrome camera. The spectral transmittances of $C = 16$ synthetic filters are of Gaussian shapes and have various FWHM values, as shown in Fig. 3(c). According to the real imaging system, the imaging noise variance is set as $\sigma_c^2 = 0.004$, where $c \in \{1, 2, \dots, C\}$, in the range $[0, 1]$. The camera response of each imaging channel is then computed according to Eq. (1).

It is of interest to illustrate the channel selection procedures of the sequential and proposed algorithms. Figure 4 shows that, when $C_S = 1$, both algorithms identify the optimal channel No. 11. When $C_S = 2$, the sequential algorithm keeps channel No. 11 and selects an additional channel No. 5, while the DE algorithm selects two novel channels, Nos. 6 and 14. When $C_S = 3$, the sequential algorithm reserves channels Nos. 11 and 5, and selects the third channel No. 15. In contrast, the DE algorithm selects channels Nos. 4, 8, and 14.

We note that the sequential algorithm is indeed a greedy search algorithm and consequently can be trapped into local minimums. Thanks to the inherent mutation operation, the proposed binary DE algorithm is able to produce a global optimal solution. Figure 5 illustrates the color accuracy with respect to various channel numbers C_S . It is observed that, in terms of both spectral rms error and color difference error, the proposed algorithm performs obviously better than the sequential algorithm when

$C_S \leq 8$. It is worth noting that, in the case of $C_S = 3$, the colorimetric error of the sequential algorithm is around $11 \Delta E_{00}$ units. This means that the three channels selected by the sequential algorithm are not acceptable for color imaging.

Table 1 shows the spectral and colorimetric errors with respect to various numbers of selected channels, C_S . The colorimetric errors are computed under three typical CIE standard illuminants, namely, D56, A, and F2. It is observed that, in terms of spectral rms error, the proposed algorithm always performs better, at least not worse, than the sequential algorithm. In quite a few cases, the proposed algorithm produces slightly higher ΔE_{00}

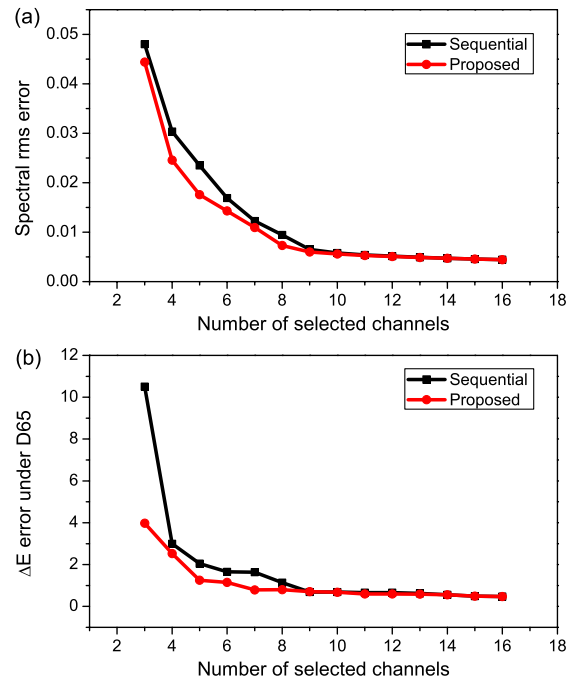


Fig. 5. (a) Spectral rms errors and (b) colorimetric ΔE_{00} errors under D65 with respect to various channel numbers.

Table 1. Average Spectral rms Errors and Color Difference Errors with Respect to Various Channel Numbers (C_S) on Synthetic Data

C_S	Sequential Algorithm				Proposed Algorithm			
	Spectral rms	ΔE_{00} (D65)	ΔE_{00} (A)	ΔE_{00} (F2)	Spectral rms	ΔE_{00} (D65)	ΔE_{00} (A)	ΔE_{00} (F2)
3	0.04801	10.508	8.947	10.016	0.04441	3.982	3.660	3.883
4	0.03037	2.995	2.898	3.290	0.02458	2.525	1.742	2.344
5	0.02350	2.047	2.247	2.409	0.01756	1.255	1.172	1.287
6	0.01692	1.658	1.523	1.905	0.01429	1.146	0.973	1.311
7	0.01227	1.639	1.509	1.891	0.01094	0.793	0.938	0.886
8	0.00946	1.135	1.148	1.418	0.00729	0.803	0.803	0.817
9	0.00650	0.689	0.632	0.723	0.00598	0.703	0.634	0.732
10	0.00580	0.684	0.634	0.699	0.00560	0.679	0.615	0.682
11	0.00542	0.659	0.613	0.640	0.00529	0.590	0.547	0.652
12	0.00516	0.661	0.610	0.643	0.00506	0.591	0.544	0.652
13	0.00492	0.625	0.603	0.640	0.00489	0.585	0.542	0.651
14	0.00472	0.559	0.535	0.593	0.00474	0.559	0.535	0.593
15	0.00456	0.492	0.469	0.530	0.00456	0.492	0.469	0.530
16	0.00446	0.477	0.443	0.507	0.00446	0.477	0.443	0.507

Table 2. Average Spectral rms Errors and Color Difference Errors with Respect to Various Channel Numbers (C_S) on Real Data

C_S	Sequential Algorithm				Proposed Algorithm			
	Spectral rms	ΔE_{00} (D65)	ΔE_{00} (A)	ΔE_{00} (F2)	Spectral rms	ΔE_{00} (D65)	ΔE_{00} (A)	ΔE_{00} (F2)
3	0.05004	11.034	9.450	10.579	0.04530	4.248	4.073	4.178
4	0.03129	3.217	3.168	3.611	0.02624	2.653	1.977	2.493
5	0.02322	1.970	2.245	2.387	0.01820	1.682	1.538	1.639
6	0.01658	1.382	1.365	1.713	0.01425	1.123	1.033	1.332
7	0.01282	1.195	1.224	1.515	0.01073	1.045	0.953	1.285
8	0.00899	1.255	1.282	1.606	0.00727	0.725	0.580	0.892
9	0.00604	0.576	0.501	0.559	0.00558	0.411	0.374	0.428
10	0.00526	0.427	0.406	0.493	0.00481	0.409	0.377	0.423
11	0.00468	0.421	0.397	0.471	0.00433	0.391	0.364	0.399
12	0.00430	0.397	0.367	0.418	0.00405	0.409	0.388	0.435
13	0.00401	0.394	0.358	0.409	0.00385	0.394	0.367	0.416
14	0.00376	0.392	0.357	0.405	0.00372	0.381	0.349	0.399
15	0.00365	0.380	0.345	0.399	0.00362	0.342	0.320	0.350
16	0.00355	0.340	0.315	0.350	0.00355	0.340	0.315	0.350

errors. This is due to the nonlinear and complicated transform between color difference and spectral reflectance.

B. Real Data

In the real data circumstance, we assume the spectral power distribution of lamps, the spectral sensitivity of the camera, and the spectral transmittances of the filters are all unknown. The spectral responsivity, which is the combination of these three terms, is mathematically estimated under the constraint of non-negativity, as discussed in Section 2.

Table 2 lists the spectral and colorimetric errors of the sequential and proposed algorithms. It is observed that, in terms of spectral rms error, the proposed algorithm performs better than the sequential algorithm in all cases. In terms of colorimetric error, the proposed algorithm performs better in most cases.

It is also found that from Table 2 that the colorimetric error of the proposed algorithm decreases rapidly in the range $C_S \in \{3, 4, \dots, 9\}$, and remains relatively stable when $C_S \geq 9$. This indicates that

$C_S = 9$ optimally selected imaging channels may be sufficient for spectral color measurement. Furthermore, for applications in which the accuracy level $\Delta E_{00} \approx 1.0$ is acceptable, only seven selected channels are necessary in the multispectral imaging

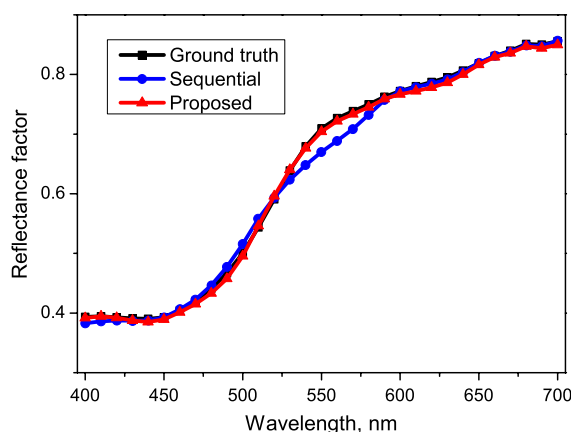


Fig. 6. Reconstruction results of a typical spectral reflectance.

system. This would greatly improve the imaging efficiency.

Figure 6 shows the reconstruction of a typical spectral reflectance using the sequential algorithm and the proposed binary DE algorithm when $C_S = 8$. It is found that the reflectance reconstructed by the proposed algorithm is more accurate.

7. Conclusion

The determination of optimal channels is an important issue for multispectral color imaging. In this paper the channel selection problem is converted to a binary optimization problem, which is solved using a novel binary DE algorithm. In the algorithm, a mutation vector is generated by a scaled differential table, and the trial vectors are produced using a self-crossover strategy. The experimental results show that the proposed algorithm performs better than the traditional sequential algorithm. It is also verified that a reduced number of imaging channels can be sufficient for practical applications.

This work was supported by the National Natural Science Foundation of China under grants 61371160, 61271339, and 61171153, the Hong Kong Research Institute of Textiles and Apparel (HKRITA) under grant ITP/009/07TP, and the Science Technology Department of Zhejiang Province under grant 2010R50006.

References

1. J. Katrasnik, F. Pemus, and B. Likar, "Radiometric calibration and noise estimation of acousto-optic tunable filter hyperspectral imaging system," *Appl. Opt.* **52**, 3526–3537 (2013).
2. H. L. Shen, J. H. Xin, and S. J. Shao, "Reflectance reconstruction for multispectral imaging by adaptive Wiener estimation," *Opt. Express* **15**, 15545–15554 (2007).
3. J. Brauers and T. Aach, "Geometric calibration of lens and filter distortions for multispectral filter-wheel cameras," *IEEE Trans. Image Process.* **20**, 496–505 (2011).
4. P. L. Vora, J. E. Farrell, J. D. Tietz, and D. H. Brainard, "Image capture: simulation of sensor responses from hyperspectral images," *IEEE Trans. Image Process.* **10**, 307–316 (2001).
5. H. Haneishi, T. Hasegawa, A. Hosoi, Y. Yokoyama, N. Tsumura, and Y. Miyake, "System design for accurately estimating the spectral reflectance of art paintings," *Appl. Opt.* **39**, 6621–6632 (2000).
6. J. Gerhardt and J. Y. Hardeberg, "Spectral color reproduction minimizing spectral and perceptual color differences," *Color Res. Appl.* **33**, 494–504 (2008).

7. J. Y. Hardeberg, "Acquisition and reproduction of color images: colorimetric and multispectral approaches," Ph.D. dissertation (Ecole Nationale Supérieure des Télécommunications, 1999).
8. V. Cheung, S. Westland, C. Li, J. Hardeberg, and D. Connah, "Characterization of trichromatic color cameras by using a new multispectral imaging technique," *J. Opt. Soc. Am. A* **22**, 1231–1240 (2005).
9. F. H. Imai, M. R. Rosen, and R. S. Berns, "Comparison of spectrally narrow-band capture versus wide-band with a priori sample analysis for spectral reflectance estimation," in *IS&T/SID Eighth Color Imaging Conference* (2000), pp. 234–241.
10. N. Shimano, "Optimization of spectral sensitivities with Gaussian distribution functions for a color image acquisition device in the presence of noise," *Opt. Eng.* **45**, 013201 (2006).
11. M. A. Lopez-Alvarez, J. Hernandez-Andres, E. M. Valero, and J. Romero, "Selecting algorithms, sensors, and linear bases for optimum spectral recovery of skylight," *J. Opt. Soc. Am. A* **24**, 942–956 (2007).
12. N. C. Hu and C. C. Wu, "Optimal selection of commercial sensors for linear model representation of daylight spectra," *Appl. Opt.* **47**, 3114–3123 (2008).
13. V. Cheung and S. Westland, "Methods for optimal color selection," *J. Imaging Sci. Technol.* **50**, 481–488 (2006).
14. H. L. Shen, H. G. Zhang, J. H. Xin, and S. J. Shao, "Optimal selection of representative colors for spectral reflectance reconstruction in a multispectral imaging system," *Appl. Opt.* **47**, 2494–2502 (2008).
15. A. Alsam and G. Finlayson, "Integer programming for optimal reduction of calibration targets," *Color Res. Appl.* **33**, 212–220 (2008).
16. K. V. Price and R. M. Storn, "Differential evolution—a simple and efficient heuristic for global optimization over continuous spaces," *J. Global Optim.* **11**, 341–359 (1997).
17. K. V. Price, R. M. Storn, and J. A. Lampinen, *Differential Evolution: A Practical Approach to Global Optimization*, 1st ed., Natural Computing Series (Springer, 2005).
18. R. S. Prado, R. C. P. Silva, F. G. Guimaraes, and O. M. Neto, "Using differential evolution for combinatorial optimization: a general approach," in *IEEE International Conference on Systems, Man, and Cybernetics* (IEEE, 2000), pp. 11–18.
19. M. H. Kashan, A. Kashan, and N. Nahavandi, "A novel differential evolution algorithm for binary optimization," *Comput. Optim. Appl.* **55**, 481–513 (2013).
20. H. L. Shen, Z. H. Zhang, C. C. Jin, X. Du, S. J. Shao, and J. H. Xin, "Adaptive characterization method for desktop color printers," *J. Electron. Imaging* **22**, 023012 (2013).
21. G. Pampara, A. P. Engelbrecht, and N. Franken, "Binary differential evolution," in *IEEE Congress on Evolution Computation* (IEEE, 2006), pp. 1873–1879.
22. M. R. Luo, G. Cui, and B. Rigg, "The development of the CIE 2000 colour-difference formula: CIEDE2000," *Color Res. Appl.* **26**, 340–350 (2001).